

# Depth effects on the flow features and noise signature of shallow cylindrical cavities at a Mach number of 0.25

O. Marsden\*, C. Bogey†, C. Bailly‡

*Laboratoire de Mécanique des Fluides et d'Acoustique*

*Ecole Centrale de Lyon & UMR CNRS 5509*

*36 avenue Guy de Collongue, 69134 Ecully cedex, France*

Flow field features and acoustic radiation around circular cylindrical cavities of 10 cm diameter and depth ranging from 1 to 10 cm under subsonic turbulent grazing flow are studied numerically at a free-stream flow velocity of  $90 \text{ m}\cdot\text{s}^{-1}$ . Computations are based on the high-accuracy resolution of the full Navier-Stokes equations, allowing the direct computation of the time-dependent sound field in and around the cavity. A description of the flow field inside the cavity is given, and compared where possible to available experimental results, yielding overall favourable comparisons. In particular, unusual features such as asymmetrical mean flow for a cavity of depth equal to half its diameter, and mean flow flapping for cavities of depth around one third of their diameter, are reproduced numerically. Acoustic spectra outside the cavity show that the shallow cavities studied here are not dominated by a depth mode resonance.

## I. Introduction

The general behaviour of cylindrical cavities subject to grazing flows is highly dependent on the ratio of their depth to diameter, which will henceforth be referred to as  $\kappa$ , defined by  $\kappa = H/D$ . Deep cavities, for which  $\kappa$  is greater than approximately four, exhibit strong acoustic resonance at discrete frequencies which are the odd multiples of the quarter wavelength depth mode. These frequencies are thus independent of the incoming flow velocity. Panpipes<sup>1</sup> and to a lesser extent flue organ pipes<sup>2</sup> are an example of this type of behaviour. For large values of  $\kappa$ , the geometry of the mouth opening plays a minimal role in frequency selection, and rectangular section cavities exhibit similar acoustic trends. Yang *et al.*<sup>3</sup> performed a detailed investigation of deep rectangular cavities, illustrating the effect of  $\kappa$ , of the Mach number as well as of the ratio of cavity length to boundary layer thickness on observed frequencies and on generated acoustic fluctuation levels. Deep cylindrical cavities have also been studied in the context of hydraulic systems, where severe coupling between flow and acoustic resonances in side branches has been observed.<sup>4-8</sup> For cylindrical cavities where  $\kappa$  is between roughly one and four, strong tonal radiation is again observed, but tone frequencies in this range of depths depend not only on cavity depth but also on flow speed. This has been observed for example in the works of Elder,<sup>9</sup> Parthasarathy,<sup>10</sup> and more recently of Marsden *et al.*<sup>11</sup> In the latter, it is shown that a semi-analytical model based on the coupling between the cavity's acoustic depth mode and shear layer forcing is able to provide a good match with experimentally observed frequencies.

---

\*Assistant professor, Ecole centrale de Lyon, email: olivier.marsden@ec-lyon.fr

†CNRS research scientist, Ecole centrale de Lyon

‡Professor at ECL & Institut Universitaire de France

For shallower cavities, the smaller depth is no longer sufficient to generate strong acoustic tones. However, the flow inside shallow cavities exhibits interesting features. and Winter<sup>12</sup> studied the drag induced by obstacles in boundary layers. They obtained precise measurements of the drag caused by various holes and protuberances placed in a flat plate boundary layer over a wide range of Mach numbers. Their work was the first to pinpoint a strong non-monotonic variation of cavity induced drag with depth in the case of cylindrical cavities. They were also the first to report the existence of an asymmetric mean flow regime for certain cavity depths, observed thanks to oil film visualisation, and they noted that cavity drag reached a maximum for depths exhibiting strong mean flow asymmetry. The most detailed study to date was performed by Hiwada *et al.*<sup>13</sup> They provided wall pressure measurements, both static and fluctuating, for cavity depth ratios between  $0.2 \leq \kappa \leq 1$ . Their static pressure measurements showed the existence of two asymmetric mean flow regimes. The first is bistable, with two stable states antisymmetrical with respect to the  $(x, z)$  plane, see figure 1. In this regime, the flow can be switched from one state to the other by perturbing the free stream conditions upstream of the cavity. This regime was observed by Hiwada for cavities of depth ratio in the range  $0.4 \leq \kappa \leq 0.6$ . In the second regime, the cavity flow hops from one asymmetrical state to the other by itself, apparently at random, albeit long, intervals. Hiwada deduced this regime from pressure recordings on the cavity wall, and referred to this behaviour as flapping. The range of depths for which flapping was observed was  $0.2 \leq \kappa < 0.4$ . More recently, Dybenko & Savory<sup>14</sup> performed hot-wire measurements in addition to static and fluctuating pressure measurements for configurations similar to those studied by Hiwada. They showed that the flow asymmetry found inside the cavity for certain depths extends well into the cavity’s wake. They also proposed that high levels of drag found for certain cavity depths might be linked to strong shear layer oscillations in these cases. Dybenko also provided a succinct experimental confirmation<sup>15</sup> of the flapping regime first observed by Hiwada. Haigermoser *et al.*<sup>16</sup> used stereoscopic and tomographic PIV to examine a cavity of depth equal to half its diameter. Their results highlight the skewed nature of the asymmetrical mean flow found for this configuration. Finally Marsden *et al.*<sup>11</sup> characterized the flow and acoustic field generated by cylindrical cavities of depth close to their diameter, and described the strong tonal depth-dependent whistling observed at certain velocities.

In this work, noise generation by flow around shallow cylindrical cavities is studied computationally. Cavities with a diameter  $D$  of 10 cm and ratios of depth to diameter  $\kappa = H/D$  ranging from 0.1 to 1 are considered, at a Mach number of 0.25 or equivalently a freestream flow velocity of  $90 \text{ m.s}^{-1}$ . The diameter-based Reynolds number of the cavity flows is 600,000, and the incoming boundary layer has a specified thickness of  $\delta/D = 0.17$ , in order to match the experimental conditions used for the study of acoustic fields around cylindrical cavities of  $1 \leq \kappa \leq 1.5$ .<sup>17</sup> For the same reason, the incoming boundary layer is perturbed to approximate the turbulent upstream conditions. This work is the continuation of previous studies by the same team, which were devoted to the study of flow and acoustics generated by deeper cavities, with depth to diameter ratios ranging from 1 to 1.5 and flow speeds in the range of  $M = 0.2$  to  $M = 0.32$ , both from an experimental point of view<sup>17</sup> and with a numerical approach.<sup>18</sup>

Such deep cavities are known to generate intense depth-dependent acoustic tones,<sup>11</sup> while the cavity depths of interest here are anticipated to be less prone to depth mode resonance. Nevertheless, given the unusual flow features found for certain depth parameters, their acoustic signature will be examined.

## II. Computational parameters and configuration details

Simulations are performed by solving the unsteady compressible Navier-Stokes equations using low-dispersion and low-dissipation finite-difference schemes.<sup>19</sup> A multi-block approach is followed, with

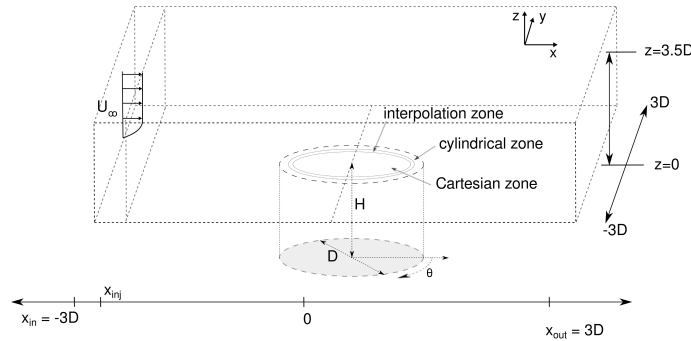
cylindrical coordinates being used to represent the circular cavity wall, and Cartesian coordinates for both the centre of the cavity and the outer flow zone. Code parallelisation is based on MPI, and where necessary, inter-grid communication is carried out via optimized interpolation.<sup>20</sup> The LES approach, referred to as LES-RF for *relaxation filtering*,<sup>21</sup> is based on the explicit application of a low-pass high-order filtering operation to the flow variables, in order to take into account the dissipative effects of the subgrid scales by relaxing turbulent energy only through the smallest discretized scales. It has been implemented with success in previous simulations of subsonic round jets,<sup>21,22</sup> airfoils<sup>23</sup> and cavities.<sup>17,24</sup> Near boundaries, and in particular near solid walls, optimized non-centred finite-difference schemes and filters are used.<sup>25</sup> In order to allow the direct computation of the noise field created by the flow, non-reflecting boundary conditions<sup>26</sup> are prescribed at free boundaries.

Figure 1 provides a sketch of the computational domain as described below. The origin of the coordinate system is located in the centre of the cavity’s upper opening. The outer computational domain covers the range  $-3.6 < x/D < 5.2$ ,  $-3.3 < y/D < 3.3$  and  $0 < z/D < 4.8$ , and is discretized by  $427 \times 270 \times 102$  points in the streamwise  $x$ , cross-stream  $y$  and vertical  $z$  directions respectively. The cavity walls are meshed by a cylindrical grid composed of  $300 \times 30$  points in the azimuthal and radial directions, and a depth-dependent number of points in the vertical direction. Finally the centre is meshed by a Cartesian grid with the same grid spacing as that used in the outer zone. A total of fourteen computations with different values of  $\kappa$  have been performed, over the range  $\kappa \in [0.1, 1]$ , see table 1.

$\kappa$	0.1	0.15	0.2	0.3	0.32	0.33	0.35	0.4	0.5	0.6	0.7	0.8	1.0
M points	1	1.6	2	2.7	2.8	2.8	2.9	3	3.1	3.4	3.7	4	4.5

**Table 1. Number of grid points, in millions, in the cavity zone of the reported computations.**

The upstream flow velocity studied here is  $90 \text{ m.s}^{-1}$ , and a boundary layer thickness of 16 mm is chosen, in order to match experimental conditions<sup>17</sup> as closely as possible for the cavity of depth ratio  $\kappa = 1$ . A turbulent mean profile based on the single equation model of Guarini<sup>27</sup> is imposed at the entry, and discretized by 30 grid points in the  $z$  direction. Slightly downstream of the entry plane at  $x/D = -3.2$ , volumetric force terms are injected in order to generate turbulent-like fluctuations in the boundary layer before it reaches the cavity. The free-stream velocity and diameter-based Reynolds numbers for these cavity flows are equal to  $\text{Re}_D = 6 \times 10^5$ . In what follows, flow components are noted  $U$ ,  $V$  and  $W$  for the mean values of the velocity field in the  $x$ ,  $y$  and  $z$  directions respectively, and  $u$ ,  $v$  and  $w$  for the corresponding instantaneous values.



**Figure 1. Sketch (not to scale) of the computational domain.**

For all cavity depths, the computations are run for a physical duration of at least 1 s, corresponding

to 700,000 time steps and nine hundred convective times across the cavity opening, and signals are recorded over the final 500,000 time steps. Cases where flapping was observed were run for a total of 1,000,000 time steps. The PSDs have been computed with a  $\delta f$  of 6 Hz, in order to present trends for very low frequencies. However, the low frequency zones of spectra should be interpreted with care, due to the small averaging resulting from this procedure.

### III. Mean flow features

In light of the dearth of experimental results available for shallow cavities, and in order to gain some idea of the validity of the computations performed for shallow cavities, results are first shown for the deepest cavity of depth ratio  $\kappa = 1$ , for which extensive experimental results have been published.<sup>11</sup>

Figures 2 (a) and (b) show profiles of mean streamwise velocity and of rms streamwise fluctuations respectively. The mean streamwise velocity is normalized by the free stream velocity, while velocity fluctuation levels are normalized by the maximum turbulence level measured in the boundary layer upstream of the cavity, of 15% both numerically and in the experiment.<sup>17</sup> Experimental data is represented by the circles, while computational data is represented by solid lines. Despite the small difference in Mach number between the two configurations, good agreement is observed, both in terms of mean velocity and in terms of streamwise fluctuations. A large confined vortex can be seen in the mean streamwise velocity plot, similar to those found in shear-driven square cavities.<sup>28,29</sup> The recirculation is intense, with a maximum downwards velocity of 30% of the free stream velocity, and a maximum velocity in the upstream direction along the cavity floor of 26 % of  $U_\infty$ . In the velocity fluctuation plot, a rapid transition from a boundary layer profile to a roughly antisymmetrical shear layer profile can be noted.

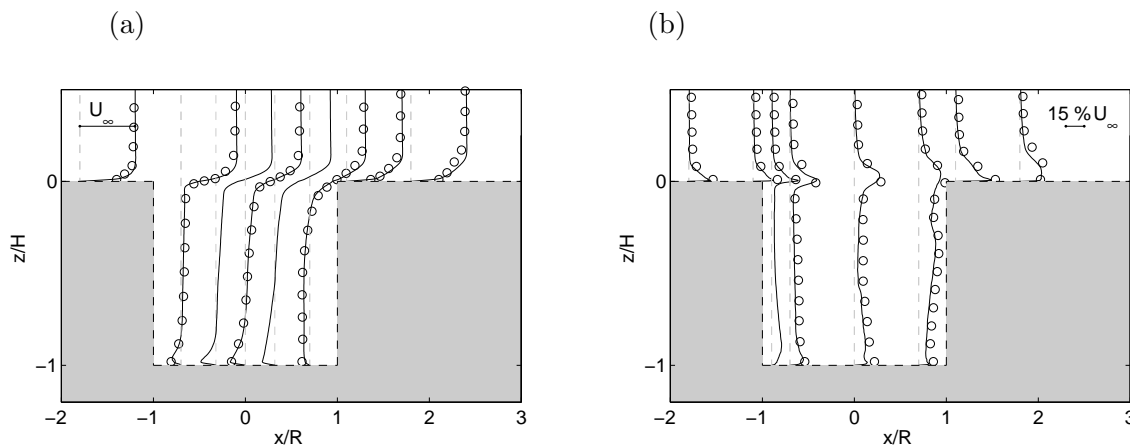


**Figure 2.** Profiles of (a) mean streamwise velocity and (b) rms values of streamwise velocity fluctuations for a cylindrical cavity of depth ratio  $\kappa = 1.0$  and diameter  $D = 2R = 10$  cm. Computational data at  $M = 0.25$  —, experimental data at  $M = 0.21$   $\circ \circ \circ$ .

A small number of experimental studies have shown that shallow cylindrical cavities exhibit bi-stable asymmetrical mean flow for depths ranging from around 0.2 to 0.6 times their diameter.<sup>13,16,30</sup> For depths close to a third of the diameter, a very low frequency flapping motion of the mean flow has also been observed.<sup>13,15</sup> The LES computations reported in this work allow a detailed examination of flow features associated with such shallow cavities. The different flow regimes reported in the literature are reproduced, at similar depth to diameter ratios.

An illustration of the asymmetry in the mean flow fields found at different depth ratios is given in figures 3 and 4, which represent the static pressure field, in non-dimensional form, on the cylindrical

wall and floor for different cavity depths.

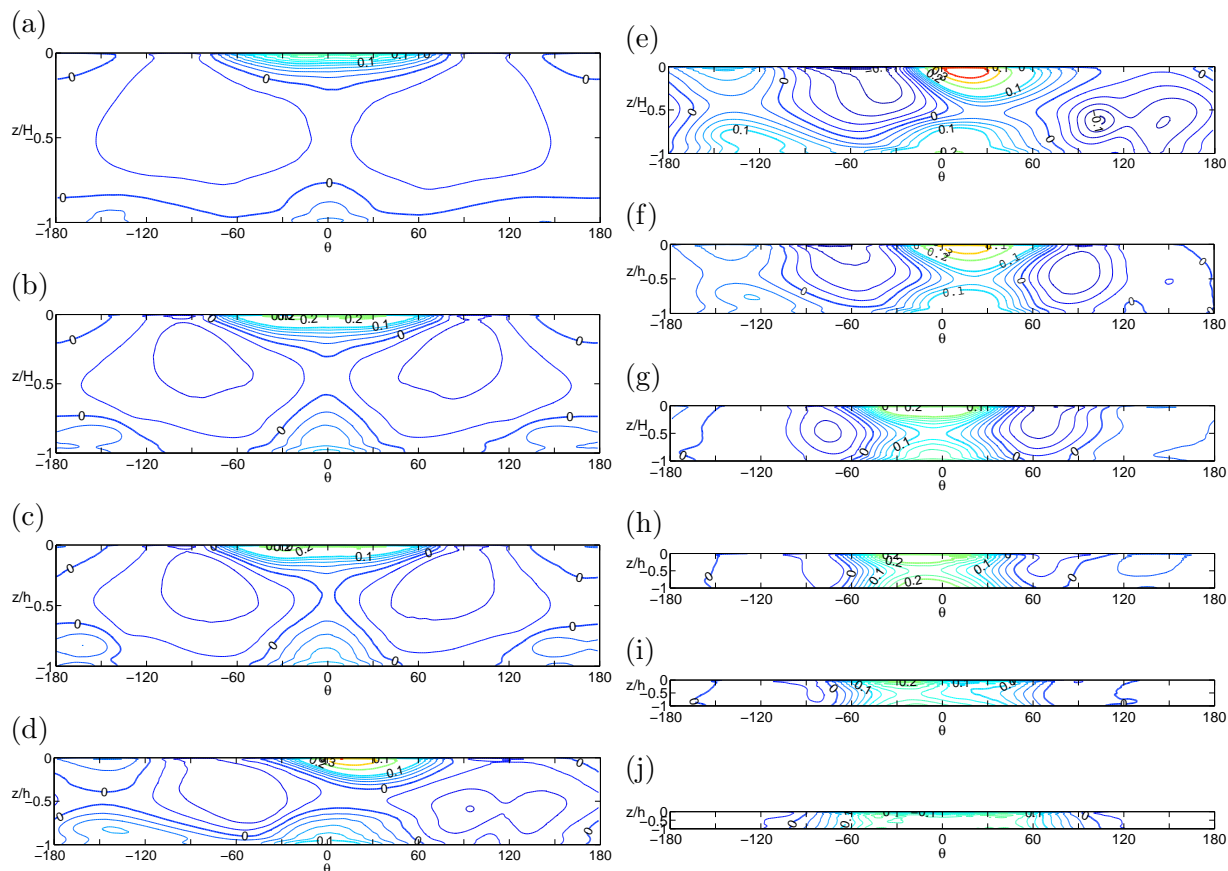


**Figure 3.** Static pressure coefficient ( $C_p$ ) distribution on the cavity wall for  $0.1 \leq \kappa \leq 1.0$ , (a)  $\kappa = 1$ , (b)  $\kappa = 0.8$ , (c)  $\kappa = 0.7$ , (d)  $\kappa = 0.6$ , (e)  $\kappa = 0.5$ , (f)  $\kappa = 0.4$ , (g)  $\kappa = 0.32$ , (h)  $\kappa = 0.2$ , (i)  $\kappa = 0.15$ , and (j)  $\kappa = 0.1$ .

The static wall pressure fields are symmetrical as intuitively expected for the deepest and shallowest of cavities, while in between, in particular for depths ratios 0.6, 0.5 and 0.4, exhibit a strong skew to one side. The same tendencies are observed on the floor pressure fields. The pressure distributions for the three largest cavity depths suggest the presence of a central recirculation occupying a large fraction of the cavity volume, as has been ascertained in an experimental investigation of deep cylindrical cavities.<sup>11</sup> The smallest depth, which is in fact inferior to the boundary layer thickness in this configuration, appears to behave much like the succession of a descending and an ascending step, as indicated by the small variation of static pressure with the depth coordinate.

For the depth ratio of  $\kappa = 0.5$  we are fortunate to have detailed wall pressure measurements to which the computational data can be compared. This is done in figures 5 (a-b) which provides the Hiwada *et al*<sup>13</sup> pressure data alongside the present numerical results shown in figures 5 (c-d) for the same depth. Although the  $C_p$  extrema are slightly less intense in the computation, a good qualitative match with the experimental pressure field is found, indicating that the general flow rotation computed from the numerical data is realistic. The pressure distribution is markedly different to that for the cavity of depth  $\kappa = 1$ , shown in figure 3 (a). It has been both rotated and distorted, and extrema are more intense. The large negative pockets of  $C_p$ , which are symmetrical in the case of the deep cavity, are now highly asymmetrical. Both pockets are rotated in the same direction by roughly  $40^\circ$ , one pocket now being centred around  $\theta = -60^\circ$  and the other centred around  $\theta = 130^\circ$ . The pocket that is closer to the downstream  $\theta = 0$  direction has shrunk, and risen to the cavity opening, while the other has dropped down to  $z/H = -0.7$  and increased in

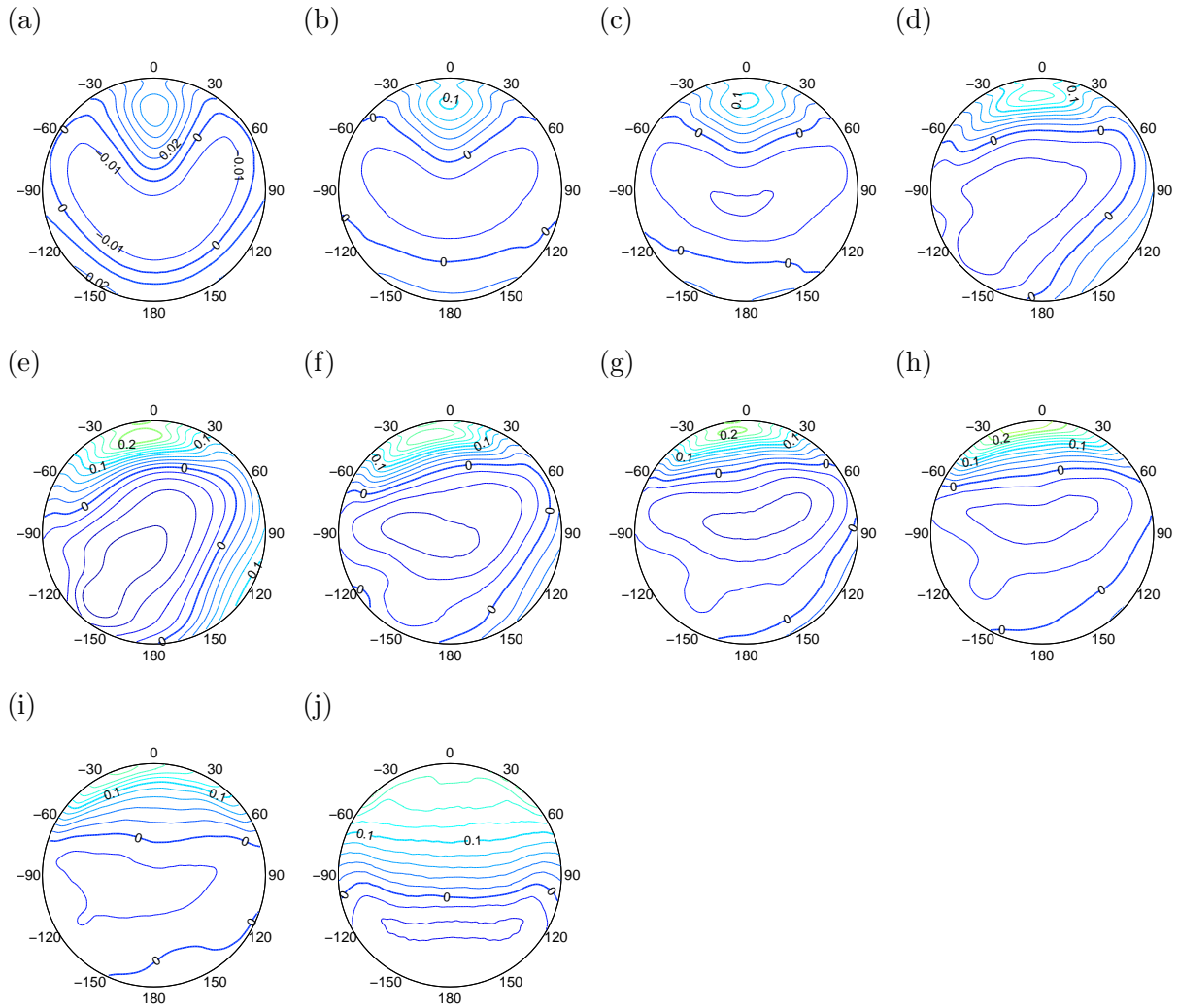
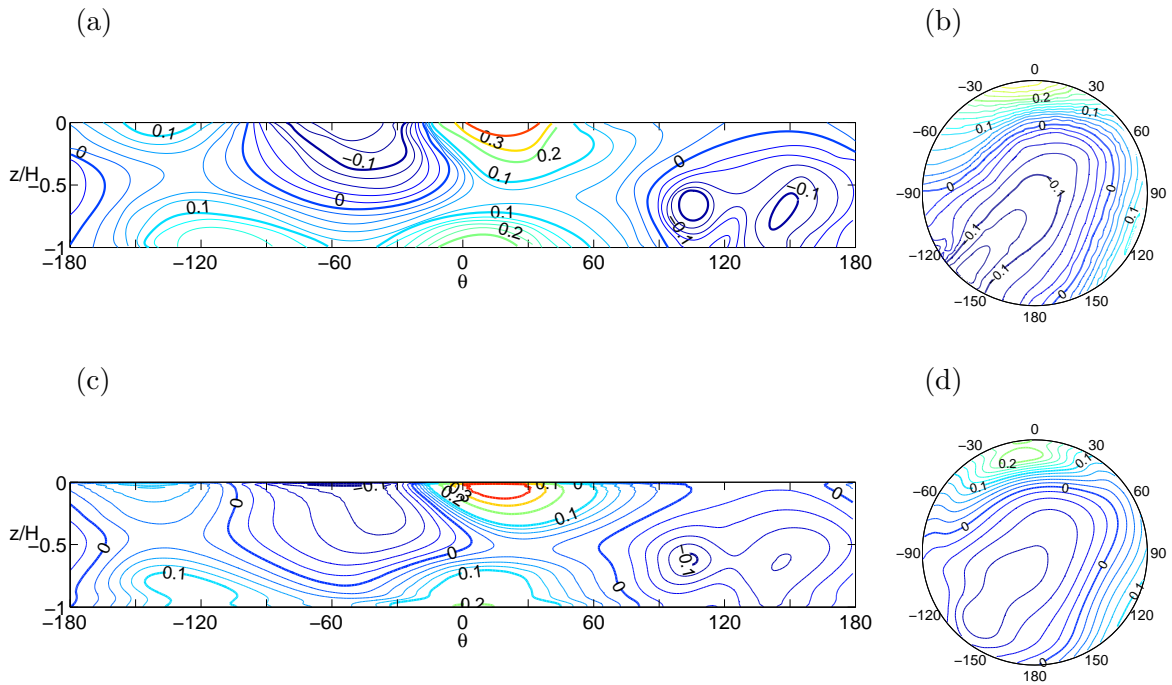


Figure 4. Pressure coefficient  $C_p$  on the cavity floor for same depths (see figure 3 caption).



**Figure 5. Static pressure coefficient on the cavity wall (left) and floor (right) for a cavity of depth  $\kappa = 0.5$ . Hiwada's data<sup>13</sup> at  $M = 0.07$  (top), and present computational data at  $M = 0.25$  (bottom).**

size. Both pockets reach negative values lower than 0.1, and are thus three to four times more intense than those of the  $\kappa = 1$  cavity. The strong positive zone of static pressure generated by the shear layer impact on the downstream cavity wall has been shifted by a little under  $30^\circ$  away from  $\theta = 0$ , and become both smaller and more intense. A maximum value of 0.52 is found in the computation, which is 2.7 times higher than the value of 0.19 obtained for the deep cavity. On the cavity floor, the pressure gradient between the downstream wall and the central zone of the cavity is much stronger than for the deep cavity, and is made up, over a wide zone, of almost parallel contours. This pressure gradient is accompanied by a substantially higher recirculation velocity along the cavity floor, reaching  $45 \text{ m}\cdot\text{s}^{-1}$  or half of the free stream velocity.

The large static pressure maximum on the cavity side wall can be better understood by examining the streamwise velocity in the  $x = 0$  plane. This quantity is represented in figure 6(a), and is strikingly asymmetrical. The shear layer descends into the cavity on the  $y > 0$  side, and is ejected into the free stream on the  $y < 0$  side, and it is this warping of the shear layer and its subsequent impact on the downstream wall which generates the strong maximum static pressure around  $\theta = 15^\circ$  visible in figure 5 (c). Figure 6(b), showing the two cross stream  $V$  and  $W$  components of the mean velocity in the  $x = 0$  plane, illustrates the cause of the shear layer warping, namely the strong rotation around the  $x$  axis which pushes the flow up for  $y < 0$  and drags it down into the cavity for  $y > 0$ . Mean flow in the cross stream  $y$  direction reaches  $0.3 \times U_\infty$ , which is of the same order of magnitude as the mean flow along the cavity floor in the streamwise  $x$  direction.

The mean flow asymmetry is better illustrated by views of the streamwise and cross-stream mean flow illustrated in figures 6 (a)-(c) for a cavity of depth ratio 0.5. The general shape of the recirculation is as expected a single large recirculation with flow heading upstream along the cavity floor, as can be ascertained from figure 6 (c), but the shear layer appears notably warped in figure 6 (a), and there is a strong cross-stream flow as can be seen in the vector plot in figure 6 b. The sideways shift in the position of the maximum static pressure described previously, visible for depth ratios around 0.5, can be attributed to this shear layer modification and the resulting impact of

high-speed fluid on the cavity wall.

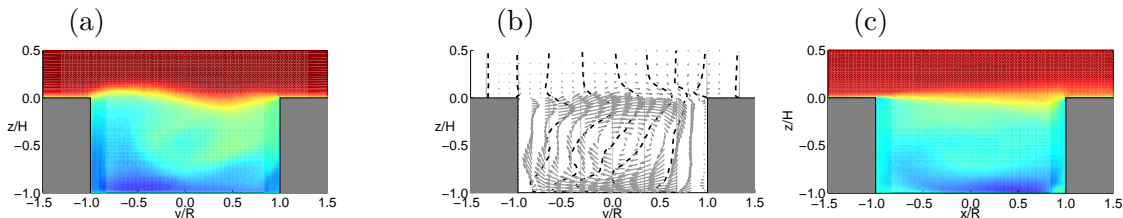


**Figure 6.** (a) Computed mean streamwise velocity and (b) cross stream velocity representation in the  $x = 0$  plane, and (c) mean streamwise velocity in the  $y = 0$  plane, for a cavity of depth  $\kappa = 0.5$ . Color scale from  $-60$  to  $90 \text{ m.s}^{-1}$  for streamwise velocity.

#### IV. Unsteady flow features and acoustics

In a second part, unsteady flow features observed in the shallow cavity computations are discussed. A behaviour that might be described as a baseline case is encountered for a cavity of depth ratio 1, presented in detail in Marsden *et al.*<sup>11</sup> Tonal acoustic radiation is observed, as are periodic vortical structures in the cavity shear layer at the same frequency. The shear layer dynamics are shown to be responsible for sustaining the acoustic depth mode resonance in such relatively deep cavities. Shallower cavities exhibit markedly different flow behaviour. The most striking of features is observed for cavities with a depth ratio between 0.2 and 0.4, reported in a very small number of experimental studies<sup>13,15</sup> to exhibit very low frequency mean flow “flapping”, or in other words sporadic switching from a mean flow skewed to one side, as in figure 6 for example, to a mean flow skewed to the other side. This behaviour appears to be reproduced in the computations for cavity depth ratios of 0.2 and 0.32.

Figure 7 illustrates this for the  $\kappa = 0.32$  computation, by representing static wall pressure as a function of time for two probe locations on the cavity downstream wall, placed symmetrically with respect to the  $y = 0$  plane. The pressure signals are presented in non-dimensional  $C_p$  form, as a function of non dimensional time  $t/T_c$  where  $T_c$  is the free stream cavity fly-over time, equal to  $1.1 \times 10^{-3}$  s in this study. The two pressure signals are in distinct phase opposition, one signal exhibiting a minimum when the other is at a maximum, and vice versa. At least three distinct time scales are visible in the pressure traces. Firstly, there are high frequency pressure fluctuations, whose time scales are linked to turbulent velocity fluctuations along the cavity walls. Secondly, the pressure signals feature notable periodic oscillations at a period of roughly 30 fly-over times. During these oscillations, the flow inside the cavity appears not to switch fully from one side to the other, since the pressure signals do not cross each other, but instead wobbles between a roughly symmetrical state and one of two asymmetrical ones. In the spectral domain, the period of these oscillations corresponds to a peak at a diameter-based Strouhal number of around 0.03. To confirm this point, the Power Spectral Density of one of the two pressure traces is presented in figure 8, scaled by the local mean squared pressure and plotted as a function of the diameter-based Strouhal number  $St_D$  and of frequency. The peak around  $St_D = 0.03$  or  $f = 27$  Hz is clearly visible, as is a peak at  $St_D = 0.12$  or  $f = 110$ . Finally, over the entire length of the recorded time signals, one large scale “flap” appears to be observed. At the beginning of the time history, the left pressure point (blue curve) is below the average value of  $C_p = 0.1$ , indicating that the large cavity recirculation is skewed to the right. At  $t/T_c = 80$ , the left and right pressure curves switch, and the right pressure curve (in black) is now below the average value, pointing to the recirculation being skewed to the left. The pressure signals switch back at  $t/T_c = 760$ , yielding an estimation of the flap time at  $\simeq 680$  convection times across the cavity, or equivalently roughly one second. It is presumed that

the true long term average of flow quantities inside the cavity is symmetrical, as is indeed suggested by the static pressure measurements performed by Hiwada *et al*<sup>13</sup> for  $\kappa = 0.37$ , which, while not perfectly symmetrical, are far more so than those performed for  $\kappa = 0.5$ . The strikingly long flap time also provides an explanation for the fact that the present computational results for cavities exhibiting this flapping behaviour seem less symmetrical than the aforementioned experimental results:<sup>13</sup> the simulation durations of around 1000 flyover times are simply not sufficient to obtain correct averages of such low-frequency flow behaviour.

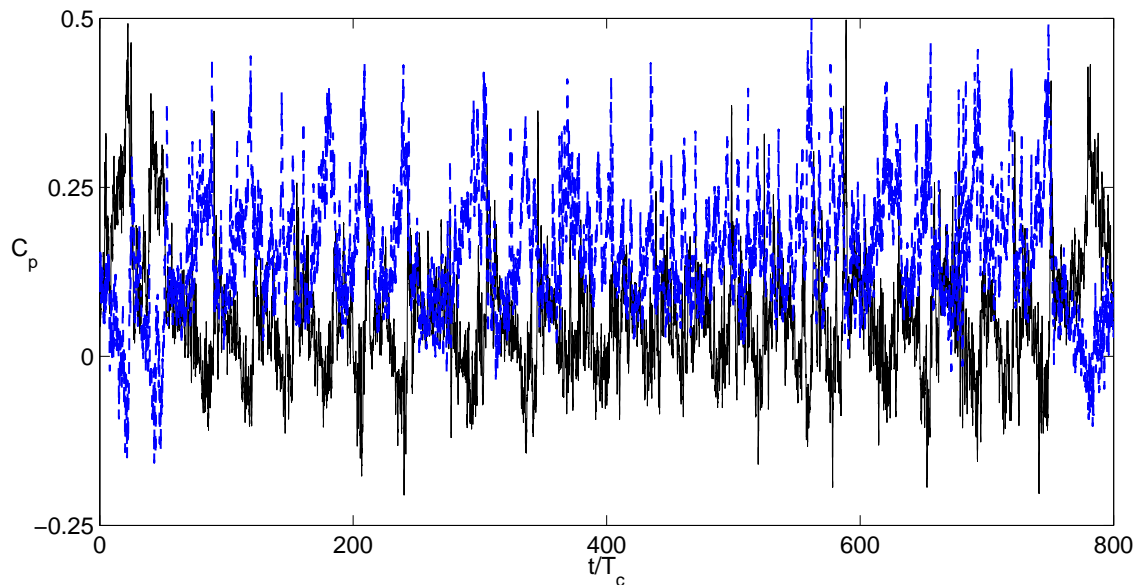


Figure 7. Computed time-dependent pressure coefficient  $C_p(t)$  at points located  $30^\circ$  to either side of the downstream  $\theta = 0$  direction, at  $z = -0.09D$  below the cavity opening. Cavity of depth ratio  $\kappa = 0.32$ .

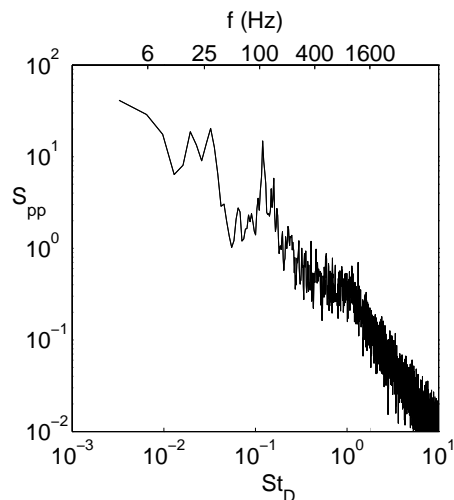
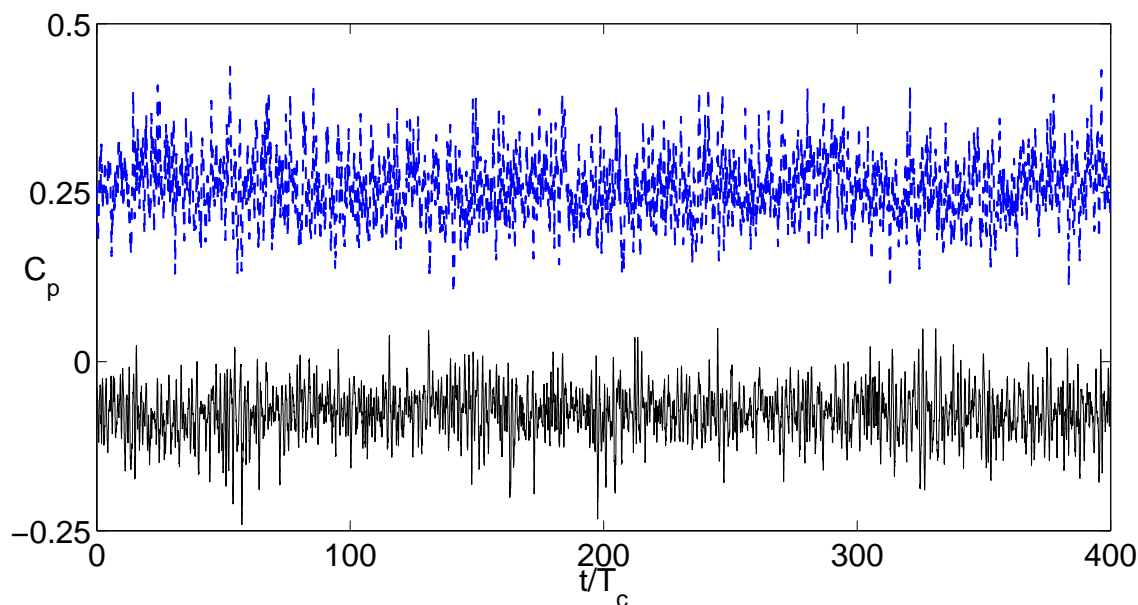


Figure 8. Power Spectral Density  $S_{pp}$  of the black signal in figure 7, scaled by the mean squared fluctuating pressure, represented as a function of the diameter-based Strouhal number  $St_D = fD/U_\infty = fT_c$  or frequency  $f$ . Cavity of depth ratio  $\kappa = 0.32$ .

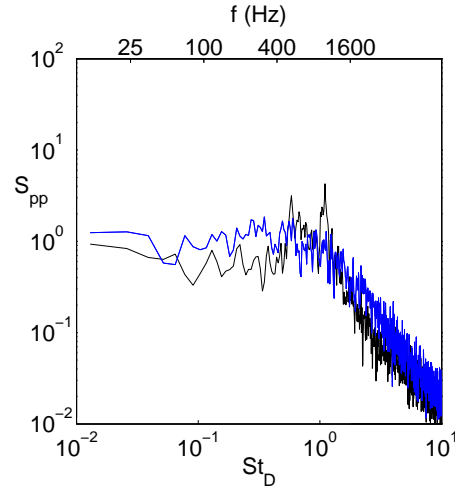
In order to illustrate the sensitivity of flow behaviour to cavity depth, the same plots are provided in figure 9 for the static wall pressure time signals recorded on the cavity downstream wall, and in

figure 10 for the corresponding PSD, for a cavity of depth ratio  $\kappa = 0.5$ . Firstly, the two pressure signals no longer have the same mean value, as was the case for the  $\kappa = 0.32$  cavity. This is consistent with the mean flow inside the cavity being asymmetric, as described in section III. The two pressure signals for this slightly deeper cavity also do not exhibit large low-frequency oscillations, instead fluctuating at high frequency around each signal's mean value. This is confirmed by the PSD of each signal, shown in figure 10, where it can be observed that the two signals contain far less low frequency content than for the  $\kappa = 0.32$  cavity, and exhibit no notable peak below approximately 400 Hz. It can be noted that the blue curve, corresponding to the signal recorded to the left of the downstream direction ( $\theta = 30^\circ$ ) contains more energy across the frequency spectrum, and also has a larger average value, than the black curve. Both of these aspects are consistent with this recording location being in the warped shear layer's impact zone on the downstream cavity wall, and on the contrary the weaker static pressure signal having been recorded in a zone where the shear layer leapfrogs the downstream wall, as discussed in section III. The black curve exhibits two distinct peaks, one at around 520 Hz, and the second at 990 Hz, which are not present in the other signal. This suggests that these frequencies are of acoustic origin, and indeed the higher frequency corresponds to the acoustic depth mode frequency of the cavity, as will be discussed with figure 13.



**Figure 9.** Computed time-dependent pressure coefficient  $C_p(t)$  at points located  $30^\circ$  to either side of the downstream  $\theta = 0$  direction, at  $z = -0.09D$  below the cavity opening. Cavity of depth ratio  $\kappa = 0.5$ .

Velocity fluctuations in the shear layer are now examined. Figures 11 (a) and (b) provide the Power Spectral Densities of horizontal  $u'$  and vertical  $w'$  velocity fluctuations in the first and second halves of the shear layer respectively, for the cavity of depth ratio 0.32, while figures 12 (a) and (b) illustrate the same quantities for the case of  $\kappa = 0.5$ . For the shallower cavity, a low frequency peak at around 30 Hz is visible both in both components of the velocity, at both upstream and downstream recording locations. This peak was already observed in the PSD of static wall pressure shown in figure 8. At the downstream location, the strongest peak for  $u'$  is observed a little above 100 Hz, also a frequency for which a peak was present in the wall pressure spectrum, see figure 8. Both  $u'$  and  $w'$  exhibit a peak at around 210 Hz, frequency at which no significant wall pressure fluctuations were observed. For the deeper  $\kappa = 0.5$  case, at the upstream location there are a number of small peaks in the range 100-1000 Hz. The most noticeable of these is observed at 590 Hz in both  $u'$  and  $w'$  signals. At the downstream recording location, the low frequency content



**Figure 10.** Power Spectral Density  $S_{pp}$  of the signals in figure 9, scaled by the mean squared fluctuating pressure, represented as a function of the diameter-based Strouhal number  $St_D = fD/U_\infty = fT_c$ . Cavity of depth ratio  $\kappa = 0.5$ .

amplitude is substantially increased, to the point where its broadband amplitude is almost equal to that of the main peak at 590 Hz. A notable wide hump has appeared around a frequency of 950 Hz on the vertical component, and to a lesser extent on the horizontal component of velocity.

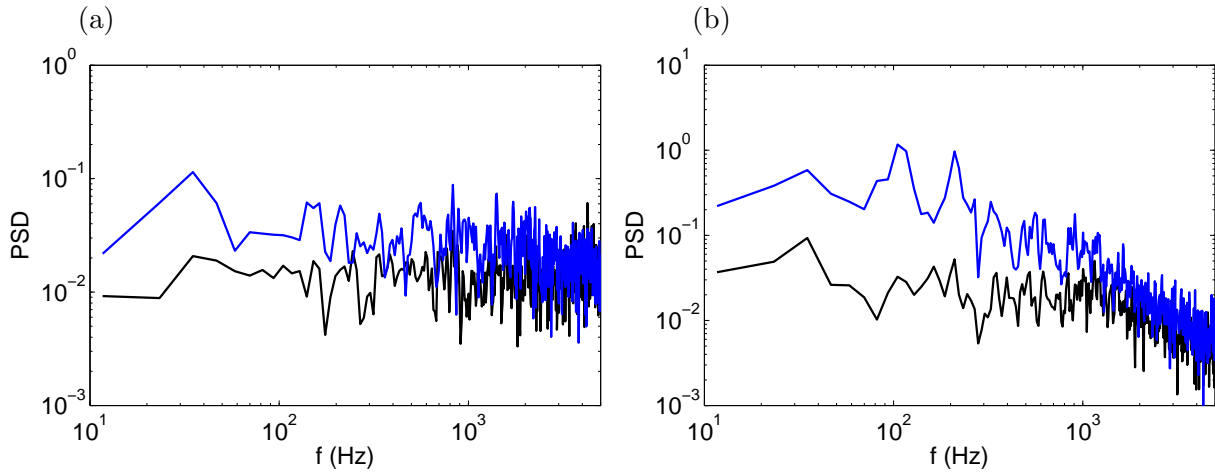


**Figure 11.** Power Spectral Densities of  $u'$  (blue curve) and  $w'$  (black curve) at (a) point  $(-0.9R, 0, 0)$  and (b) point  $(0.9R, 0, 0)$ . Cavity of depth ratio  $\kappa = 0.32$ .

Figures 13 (a) to (c) provides the acoustic signatures of cavities of depth ratios 0.2, 0.32 and 0.5 respectively. Of note is that contrary to deeper cavities with a depth ratio of one or greater, the acoustic depth mode frequency, indicated by the vertical red line in the figures, is not the main contributor to radiated sound. For depth ratios of 0.32 and 0.5, the depth mode frequency is nevertheless visible in the spectra, although far less intense than the hump between roughly 1000 and 1500 Hz present for the three cases. For the cavity of depth ratio  $\kappa = 0.5$ , a frequency very close to the depth mode of 933 Hz was already observed in the wall pressure spectrum, see figure 10. A second interesting point is that the two previously described low frequencies in the switching cavity ( $\kappa = 0.32$ ), visible as peaks at  $St_D = 0.03$  or 27 Hz and  $St_D = 0.12$  or 110 Hz in the wall pressure PSD, are not detected in the far acoustic field. However, the slight humps visible in the

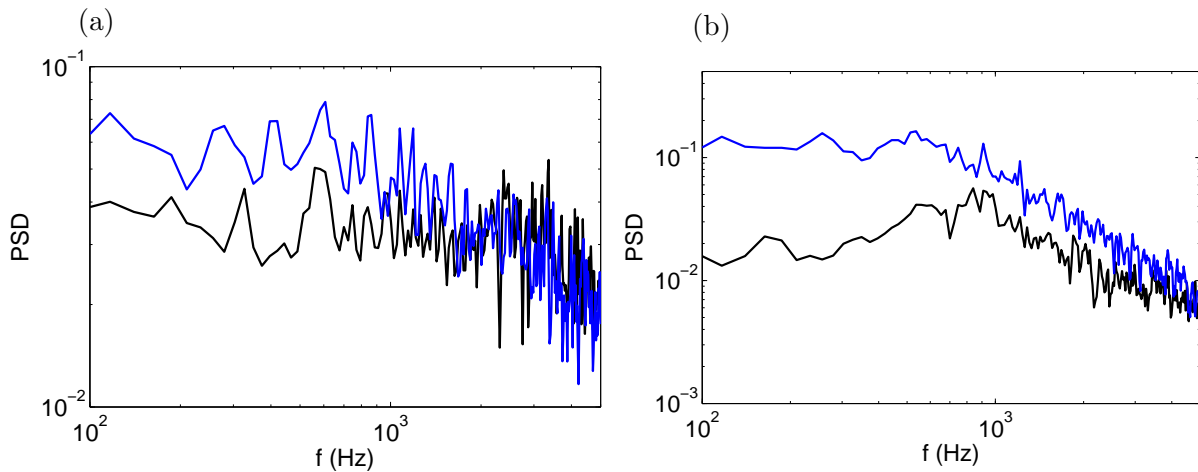


**Figure 12.** Power Spectral Densities of  $u'$  (blue curve) and  $w'$  (black curve) at (a) point  $(-0.9R, 0, 0)$  and (b) point  $(0.9R, 0, 0)$ . Cavity of depth ratio  $\kappa = 0.5$ .

wall pressure PSD around  $St_D = 0.55$  and  $St_D = 1.1$  corresponding to frequencies of 500 and 1000 Hz respectively, and in particular the second of the two, are in frequency range for which the acoustic radiation also exhibits its peak. This suggests that contrary to the case of deeper cavities, the vortical structures in the shear layer for a depth ratio of 0.32 generate sound thanks to their direct impact on the downstream cavity wall rather than thanks to their interaction with the cavity depth mode. It therefore does not come as a surprise to observe that correlation between velocity fluctuations in the shear layer and the radiated acoustic field is high, as shown in figure 14 which plots the cross correlation of vertical velocity fluctuations upstream of the cavity wall and the acoustic field above the cavity. A strong negative peak of 0.2 is observed for the expected non-dimensional delay of 1 corresponding to an “acoustic” time delay.

For the cavity of depth ratio 0.5, the high frequency hump in the acoustic PSD not directly attributable to depth resonance is particularly strong, and presents a distinct peak at 1770 Hz or  $St_D = 1.97$  whose origin is unclear. This frequency is not notable in the velocity spectra presented in figure 12 (b). Other authors have suggested that non-depth related tones<sup>15,30</sup> might be of fluid-resonant origin. If this were the case, the shear layer at the upstream cavity edge should be correlated to the forcing pressure difference across the shear layer. A first examination of this is provided in figure 15, which represents the correlation between the pressure jump across the shear layer at the upstream cavity edge and the vertical velocity fluctuations in the shear layer immediately downstream of the edge. A non-negligible correlation of -0.15 is noted for a near-zero delay of  $\tau = 2.3 \times 10^{-4}$  s, suggesting that the shear layer dynamics are indeed in part forced by the pressure difference near the upstream wall. The standard Rossiter formula  $St_D = (n - \alpha) / (U_\infty / U_C + M)$  based on the cavity diameter, with standard values of 0.25 and 0.6 for  $\alpha$  and  $(U_\infty / U_C)$  respectively, provides the Strouhal numbers  $St_D = 0.29, 0.91, 1.43, 1.95$  for  $n = 1 \dots 4$ . The Strouhal number of 1.97 could be thus due to a mode 4 in the shear layer, predicted at a Strouhal number of 1.95 with the standard Rossiter formula although no other signs of a mode 4 have been detected and the presence of such a high mode number seems unlikely.

### Concluding remarks

Computations of the flow in and around shallow cylindrical cavities have been presented. The general trends observed experimentally for such flows are captured in the computations. Random mean flow unsteadiness, one of the more unusual features of cylindrical cavity flow observed for a

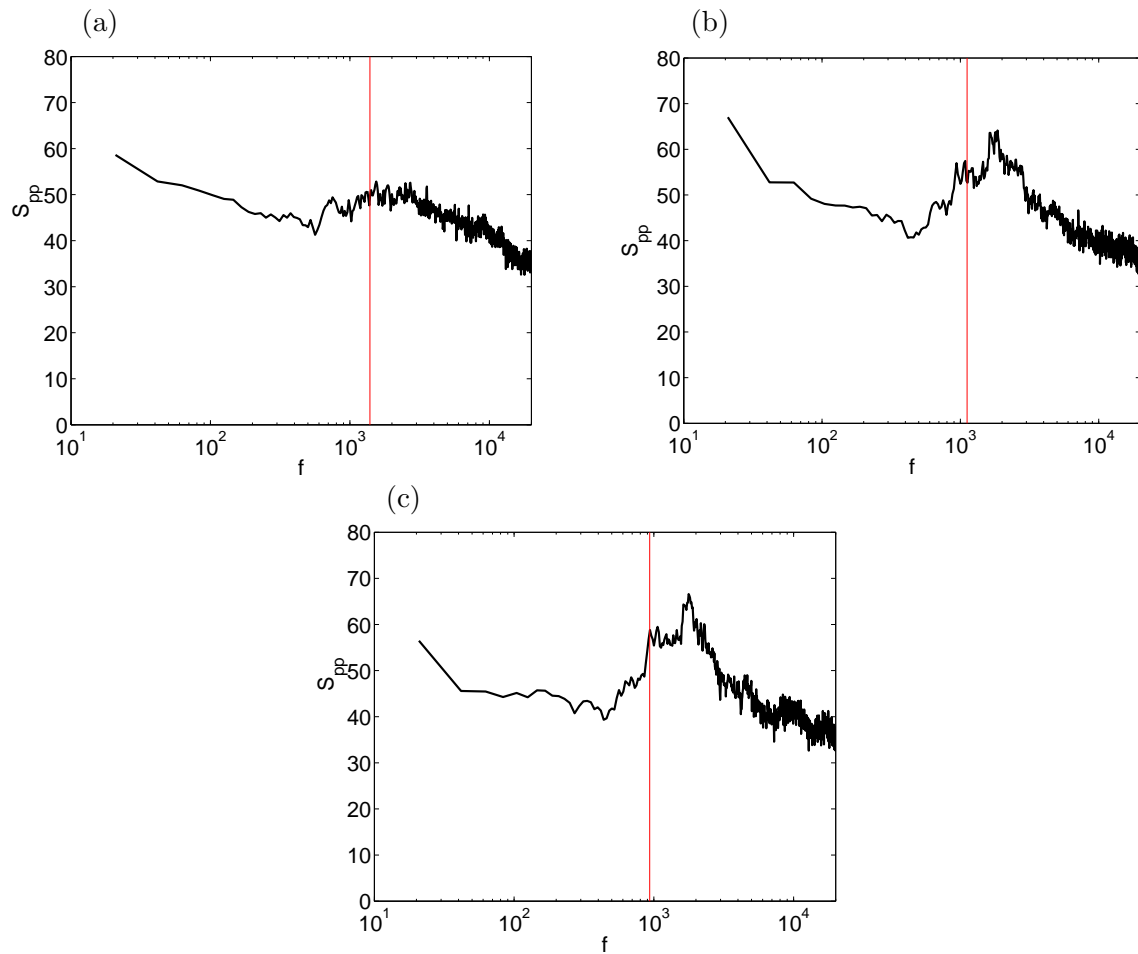


Figure 13. Pressure signal recorded 1.5 diameters above the centre of the cavity, for cavities of depth ratio (a)  $\kappa = 0.2$  (b)  $\kappa = 0.32$  and (c)  $\kappa = 0.5$ . Vertical red line corresponds to acoustic depth mode frequency computed according to  $f = h/4d_c$  with  $d_c$  cavity depth corrected according to Nomura.<sup>31</sup>

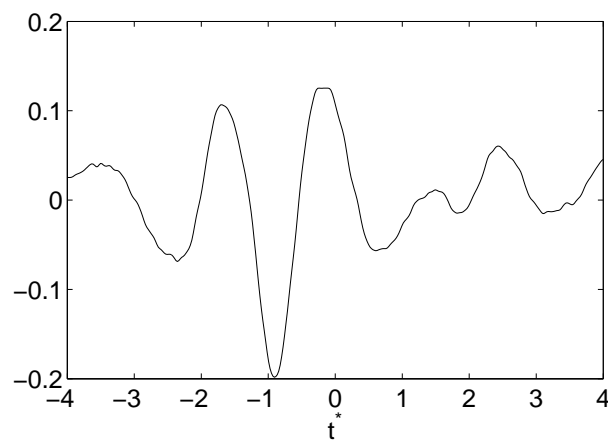
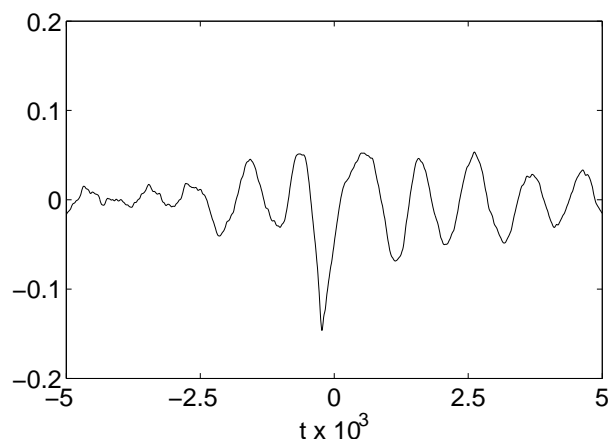


Figure 14. Cross correlation between vertical velocity fluctuation in the shear layer at  $w'(0.7R, 0, 0)$  and pressure radiated above the cavity  $p'(0, 0, 3H)$  for cavity with  $\kappa = 0.32$ , as a function of delay normalised by the sum of shear layer convection time to the downstream edge and acoustic propagation time from the wall to the pressure recording location.



**Figure 15.** Cross correlation between vertical velocity fluctuation in the shear layer  $w'(-0.95R, 0, 0)$  and the pressure jump across the shear layer at the upstream edge, for  $\kappa = 0.5$ , as a function of delay.

small range of cavity depths, appears also to be present in the computations. The acoustic field generated by such shallow cavities seems no longer to be dominated by the cavity depth mode. Nevertheless, a tonal component is still visible for certain depths, which might be due to Rossiter-like feedback in the shear layer.

### Acknowledgments

This research project is supported by the *Fondation de Recherche pour l'Aéronautique & l'Espace (FRAE)* under the contract reference AFB AEROC AV, and in collaboration with following french laboratories: ONERA, SINUMEF, IUSTI and INRIA. The team was granted access to the HPC resources of the Institut du Développement et des Ressources en Informatique Scientifique (IDRIS) under the allocation 2010-020204 made by GENCI (Grand Equipement National de Calcul Intensif).

### References

- <sup>1</sup>Fletcher, N., "Stopped-pipe wind instruments: Acoustics of the panpipes," *J. Acoust. Soc. Am.*, Vol. 117, No. 1, 2005, pp. 370–374.
- <sup>2</sup>Coltman, J., "Jet drive mechanisms in edge tones and organ pipes," *J. Acoust. Soc. Am.*, Vol. 60, No. 3, 1976.
- <sup>3</sup>Yang, Y., Rockwell, D., Lai-Fook Cody, K., and Pollack, M., "Generation of Tones Due to Flow past a Deep Cavity: Effect of Streamwise Length," *Tech report LM-06K055*, 2006.
- <sup>4</sup>Rockwell, D. and Naudascher, E., "Review - Self-sustaining oscillations of flow past cavities," *ASME Journal of Fluids Engineering*, Vol. 100, 1978, pp. 152–165.
- <sup>5</sup>Howe, M., "The dissipation of sound at an edge," *Journal of Sound and Vibration*, Vol. 70, No. 3, 1980, pp. 407–411.
- <sup>6</sup>Bruggeman, J., *Flow-induced pulsations in pipe systems*, Phd. thesis, Eindhoven University of Technology, 1987.
- <sup>7</sup>Jungowski, W., Botros, K., and Studzinski, W., "Cylindrical side-branch as tone generator," *Journal of Sound and Vibration*, Vol. 131, No. 2, 1989, pp. 265–285.
- <sup>8</sup>Ziada, S. and Shine, S., "Strouhal numbers of flow-excited acoustic resonance of closed side branches," *J. Fluids Struct.*, 1999.
- <sup>9</sup>Elder, S., "Self-excited depth-mode resonance for a wall-mounted cavity in turbulent flow," *J. Acoust. Soc. Am.*, Vol. 64, No. 3, 1978, pp. 877–890.
- <sup>10</sup>Parthasarathy, S., Cho, Y., and Back, L., "Sound generation by flow over relatively deep cylindrical cavities," *J. Acoust. Soc. Am.*, Vol. 78, No. 5, 1985, pp. 1785–1795.
- <sup>11</sup>Marsden, O., Bailly, C., Bogey, C., and Jondeau, E., "Investigation of flow features and acoustic radiation of a round cavity," *Journal of Sound and Vibration*, Vol. 331, No. 15, 2012, pp. 3521.

- <sup>12</sup>Gaudet, L. and Winter, K., “Measurements of the Drag of Some Characteristic Aircraft Excrescences Immersed in Turbulent Boundary Layers,” Tech. Rep. TM AERO 1538, Royal Aircraft Establishment, 1973.
- <sup>13</sup>Hiwada, M., Kawamura, T., Mabuchi, I., and Kumada, M., “Some characteristics of flow pattern and heat transfer past a circular cylindrical cavity,” *Bulletin of the JSME*, Vol. 26, No. 220, October 1983, pp. 1744–1752.
- <sup>14</sup>Dybenko, J. and Savory, E., “An experimental investigation of turbulent boundary layer flow over surface-mounted circular cavities,” *Jour. Aerospace Eng.*, Vol. 222, No. 1, 2008, pp. 109–125.
- <sup>15</sup>Dybenko, J., *An experimental investigation of turbulent boundary surface-layer flow over surface-mounted circular cavities*, Ph.D. thesis, The University of Western Ontario, 2005.
- <sup>16</sup>Haigermoser, C., Scarano, F., and Onorato, M., “Investigation of the flow in a circular cavity using stereo and tomographic particle image velocimetry,” *Experiments in Fluids*, Vol. 46, No. 3, 2009, pp. 517–526.
- <sup>17</sup>Marsden, O., Jondeau, E., Souchotte, P., Bailly, C., Bogey, C., and Juvé, D., “Investigation of flow features and acoustic radiation of a round cavity,” *AIAA Paper 2008-2851*, 2008.
- <sup>18</sup>Marsden, O., Bogey, C., and Bailly, C., “Numerical investigation of flow features and acoustic radiation around a round cavity,” *AIAA Paper 2010-3988*, 2010.
- <sup>19</sup>Bogey, C. and Bailly, C., “A family of low dispersive and low dissipative explicit schemes for noise computations,” *Journal of Computational Physics*, Vol. 194, No. 1, 2004, pp. 194–214.
- <sup>20</sup>Desvigne, D., Marsden, O., Bogey, C., and Bailly, C., “Development of non-centered wavenumber-based optimized interpolation schemes with amplification control for overlapping grids,” *Society for Industrial and Applied Mathematics*, Vol. 32, No. 4, 2010, pp. 2074–2098.
- <sup>21</sup>Bogey, C. and Bailly, C., “Turbulence and energy budget in a self-preserving round jet: direct evaluation using large-eddy simulation,” *Journal of Fluid Mechanics*, Vol. 627, 2009, pp. 129–160.
- <sup>22</sup>Bogey, C. and Bailly, C., “Large Eddy Simulations of transitional round jets : influence of the Reynolds number on flow development and energy dissipation,” *Physics of Fluids*, Vol. 18, 2006, 065101.
- <sup>23</sup>Marsden, O., Bogey, C., and Bailly, C., “Direct Noise Computation of the Turbulent flow around a zero-incidence airfoil,” *AIAA Journal*, , No. 4, 2008, pp. 874–883.
- <sup>24</sup>Marsden, O., Gloerfelt, X., and Bailly, C., “Direct noise computation of adaptive control applied to a cavity flow,” *C. R. Acad. Sci.*, Vol. 331, 2003, pp. 423–429.
- <sup>25</sup>Berland, J., Bogey, C., Marsden, O., and Bailly, C., “High-order, low dispersive and low dissipative explicit schemes for multiple-scale and boundary problems,” *Journal of Computational Physics*, Vol. 224, 2007, pp. 637–662.
- <sup>26</sup>Bogey, C. and Bailly, C., “Three-dimensional non-reflective boundary conditions for acoustic simulations : far field formulation and validation test cases,” *Acta Acustica*, Vol. 88, No. 4, 2002, pp. 463–471.
- <sup>27</sup>Guarini, S. E., Moser, R. D., Shariff, K., and Wray, A., “Direct numerical simulation of a supersonic turbulent boundary layer at Mach 2.5,” *Journal of Fluid Mechanics*, Vol. 414, No. 1, 2000, pp. 1–33.
- <sup>28</sup>Kistler, A. and Tan, F., “Some properties of turbulent separated flows,” *The Physics of Fluids Supplement Boundary Layers and Turbulence*, 1967, pp. S165–173.
- <sup>29</sup>O’Brien, V., “Closed streamlines associated with channel flow over a cavity,” *Physics of Fluids*, Vol. 15, No. 12, 1972, pp. 2089–2097.
- <sup>30</sup>Dybenko, J. and Savory, E., “An experimental investigation of turbulent boundary layer flow over surface-mounted circular cavities,” *CSME Forum*, 2006.
- <sup>31</sup>Nomura, Y., Yamamura, I., and Inawashiro, S., “On the acoustic radiation from a flanged circular pipe,” *J. Phys. Soc. Jap.*, Vol. 15, No. 3, 1960.